# Improving Velocity Model Using Double Parabolic RMO Picking (ModelC) and Providing High-end RTM (RTang) Imaging for OML 79 Shallow Water, Nigeria

**Osimobi, J. C, Ekemezie, I., Obobi O., Uraechu D. and Magnus K.**
Shell Petroleum Development Company of Nigeria

## ABSTRACT

Higher-order double parabolic moveouts were picked in azimuthal direction to account for the velocity variations in the Residual Moveout (RMO). The picks were then inverted using conventional Travel Time Tomography (TTI) workflow. This resulted in robust velocity model; moving from Model B to Model C, shows more realistic geological details. Sonic log (DT) also indicated that Model C was an improved Model compared to Model B. The seismic imaging approach was using the Reverse Time Migration (RTM) algorithm for BASE RTMIG image and then used the RTANG (entailed Compute angle and azimuth from local subsurface-offset analysis and reflector dips, write image, angle, azimuth volumes to disk) option to select optimum REFLECTION angle for optimum stacking, and the DSSRT post migration provided a noise filtered version of the BASE RTMIG image. Further post-stack operations like Dip Filter (DIP_FLT) were applied to better the Signal/Noise ratio. Combining the velocity model building approach (from Model A to C) and the imaging technique gave rise to an improved imaging resulting in a better definition of structural and stratigraphic features within the field. This seismic is aiding well planning and exploration maturation process. Pre-processing included Noise attenuation, De-multiple, Deconvolution, and amplitude balancing.

**Keywords:** Velocity Model, Residual Moveout, Reverse Time Migration, Travel time Tomography, Dip Filtering, Amplitude Balancing,

## INTRODUCTION

The Tertiary age Niger Delta siliclastic sediment deposits are classified into three lithostratigraphic units namely Akate, Agbada and Benin formations. The Benin formation consists of massive deposits of mainly alluvial and upper coastal plain sands (up to 2000m thick) with a few shale interbeds. This continental latest Eocene to Recent deposit is on top of Agbada formation that consists of alternating sequences of sandstone and shales with sand-shale ratio decreasing with depth, (Shell Technical Report, 2020). Most of the hydrocarbon reservoirs in the Niger Delta have been found in sandstones of the Agbada Formation, where they are trapped in rollover anticlines fronting growth faults in channels and barrier sandstone bodies.

The major petroleum-bearing unit is over 3700m thick and began in the Eocene and continues into the recent. The deeper Akata Formation is the basal unit of the Tertiary Niger Delta complex and is composed predominantly of thick shale sequences (potential source rock), turbidite sands (potential reservoirs in deep water) and minor amounts of clay and silt. It is estimated that the formation is up to 7000m thick. The Akata formation underlies the entire delta and is typically over-pressured.

The deposition of the three formations occurred in each of the five-off lapping siliclastic sedimentation cycles that comprise the Niger Delta, (Tuttle *et al.,* 1999). These cycles (depobelts) are 30-60 km wide, prograde from NW to SW direction over the oceanic crust into the Gulf of Guinea and are defined by syn-sedimentary faulting that occurred in response to variable rates of subsidence and sediment supply. The interplay of subsidence and sediment supply resulted in the deposition of 5 discrete depobelts. Each depobelt is bounded with another depobelt via huge growth faults, (Shell Technical Report, 2020).

## METHODOLOGY

Pre-processing included Noise attenuation, De-multiple, Deconvolution, and amplitude balancing. Pre-processing is very key to the success of the imaging as this step compensates for the imprints and energy loss associated with acquisition. Details of the steps can be found below.



The authors acknowledge the contributions of reviewers/assurers who clarified the work and paper. Special thanks to SPDC and JV partners for the permission to present and publish this paper and Mr. Jake Emakpor, Geoscience Manager, Shell Petroleum Development Company of Nigeria.

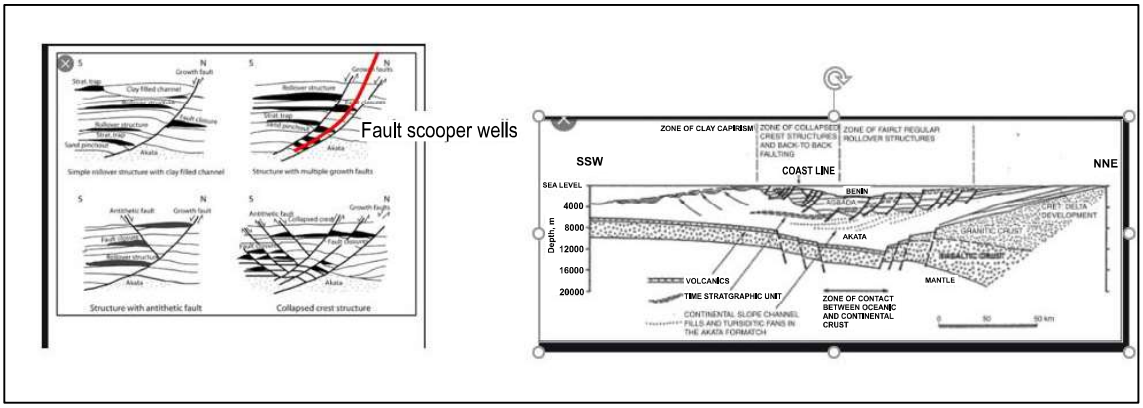


**Figure 1:** Cartoon Examples of Niger Delta oil field structures and associated trap types (left-hand side). The red line mimics fault scooper well which is a deviated well penetrating a number of accumulated hydrocarbon reservoirs. The cartoon at the right-hand side shows the key formations (i.e. Benin, Agbada and Akata) and typical presence of listric growth faults.

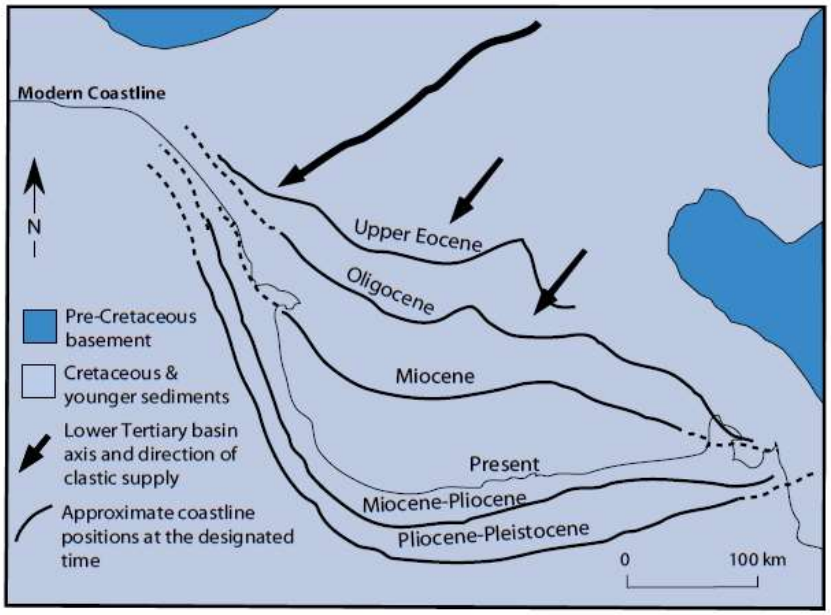


**Figure 2:** Cartoon showing a top of the progaded Niger Delta since 35 Ma with the modern coastline. The delta has advanced seaward over 200km and has broadened from a width less then 300km to a width of about 500km. The dotted lines approximate the depobelt boundaries (older coastline positions).

## NOISE ATTENUATION

Noise is any unwanted signal. It is ubiquitous. We primarily have two types: coherent (ground roll, power line noise etc.) and incoherent noise (wind, ocean waves etc.), (Shell Technical Report, 2012). Noise attenuation challenges have kept geophysicists busy for many years. Progress have been made but total elimination remains an elusive goal – hence attenuation. There are two main approaches to attenuate noise: prediction & subtraction and filtering. In the refraction FWI as in this case, our focus (primaries as it were) is to preserve the REFRACTION/Diving energy, (Shell Technical Report, 2015).

### Residual Anomalous High Amplitude Removal

Low frequency preserving de-noising was applied using an operation which handles localized anomalous amplitudes. with mixing (pseudo stack) applies a spatial filter for noise suppression and anti-aliasing protection at different frequency sub-bands.

## DECONVOLUTION

The recorded seismogram can be modelled as a convolution of the earth's impulse response with the seismic wavelet. This wavelet has many components, including source signature, recording filter, surface

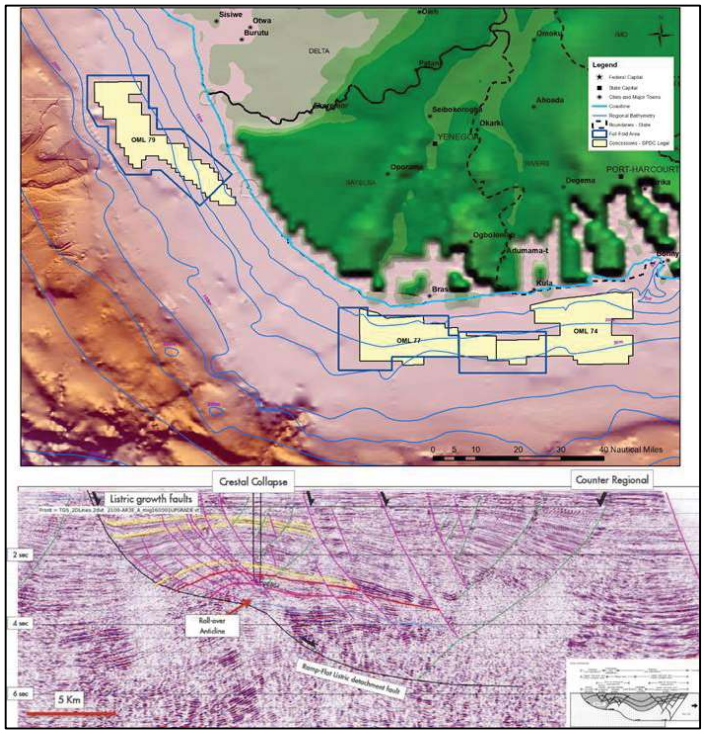


**Figure 3:** The Shallow water area is also highly characterized with structural complexities (see fig above) which poses imaging challenges in the area.

reflections, and receiver-array response, (Shell Technical Report, 2015). The impulse response comprises primary reflections (reflectivity series) and all possible multiples. Deconvolution is a filtering process which removes a wavelet from the recorded seismic trace by reversing the process of convolution.

Deconvolution is a process that counteracts this previous

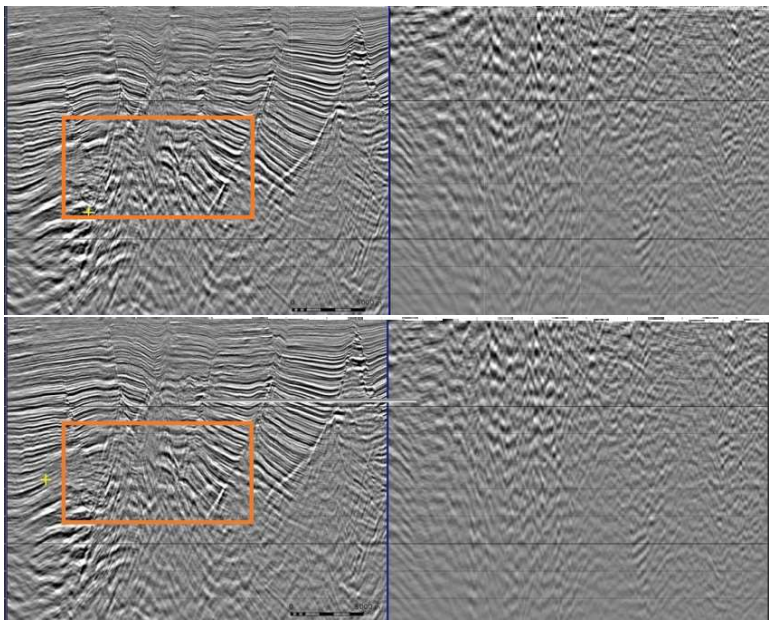

**Figure 4:** Deconvolution outcome and quality check; before deconvolution (top picture) with corresponding autocorrelation and after deconvolution (bottom picture) with corresponding autocorrelation.

convolution action. It compresses the basic wavelet in the recorded seismogram, attenuates reverberations and short-period multiples, thus increases temporal resolution, and yields a representation of subsurface reflectivity, (Shell Technical Report, 2012). The earth's impulse response is what would be recorded if the wavelet were just a spike. Therefore, the aim of this process is to convert every occurrence of the seismic wavelet in the data to an equivalent spike to obtain the earth's impulse response.

The deconvolution filter was derived on 1 trace within a time gate of 750ms – 2500ms and it was applied on the whole record length of each trace individually. This operator is applied to the input dataset, and the prediction thus obtained is then subtracted from the input data; Gap=32, Operator length= 200. Gapped deconvolution was performed by deriving an optimal single gap prediction operator via the Wiener-Levinson algorithm.
After deconvolution application, an autocorrelation was computed to QC the deconvolution and results of the reverberations since spiking deconvolution suppresses multiples. Figure 4 below shows the results before and after deconvolution, stacks, and their corresponding autocorrelations. As can be observed, reverberations are reduced after deconvolution, multiples attenuated and focusing enhanced.

**Amplitude Balancing**
Often times due to operations and or terrain challenges, anomalously high amplitudes at localized areas could be observed on a seismic dataset, (Shell Technical Report, 2010). This can be observed on a time slice as shown in figure below. Correcting for this artifact is very critical for quantitative AVO interpretations. These anomalies could be misleading to be interpreted as a fluid effect in an Amplitude vs Offset (AVO) analysis. The correction was done, and the result is as shown below.

different azimuths, rather than conventional linear RMO picking that is conducted independently along different azimuths, we applied areal double-parabolic picking.

Higher-order double parabolic moveouts were picked in azimuthal direction to account for the velocity variations in the Residual Moveout (RMO character. These picks were inverted using Travel Time Tomography (TTI). This resulted in robust velocity model, a move from Model B to Model C shows more realistic geologic details.

In DBLPAR, the moveout is fit to a second-order equation.

$$T(d_1,d_2)=T(0,0)+D_1d_1+D_2d_2+D_3d_1^2+D_4d_2^2+D_5d_1d_2$$

where the two variables d1 and d2 are XDISTX and XDISTY, respectively. The coefficients that are obtained from the picking algorithm are T (0,0) -- the migrated time at zero offset: D1,2--the first order coefficients, and D3,4,5 --the second-order coefficients

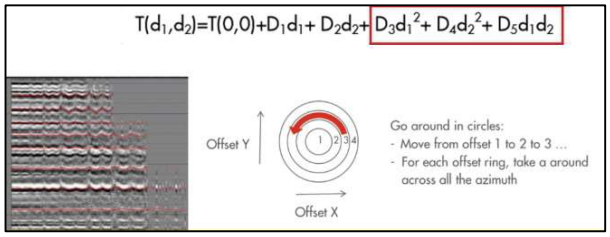


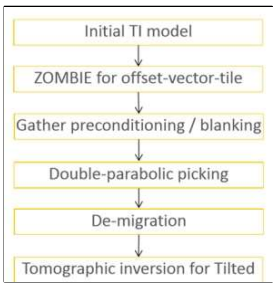


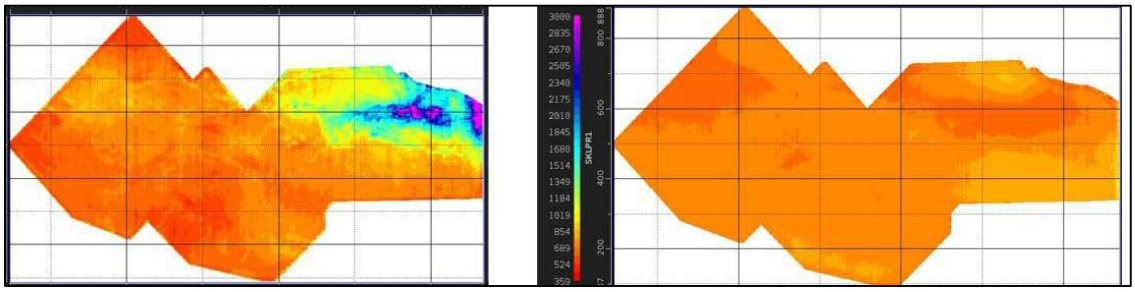

**Figure 5a:** Shot amplitude balancing. Left (before amplitude balancing) and right (after amplitude balacing)

**VELOCITY PARABOLIC PICKING**
In Ocean Bottom Node (OBN) standard tilted TI models cannot flatten the post-migration common image gathers (CIGs) along all the azimuths, and even conflicting RMO (positive along one azimuthal direction while negative along the perpendicular) exist for a single event along

The seismic imaging approach was using the Reverse Time Migration (RTM) algorithm for BASE RTMIG image and then used the RTANG (entailed Compute angle and azimuth from local subsurface-offset analysis and reflector dips, write image, angle, azimuth volumes to disk) option to select optimum REFLECTION Angle for

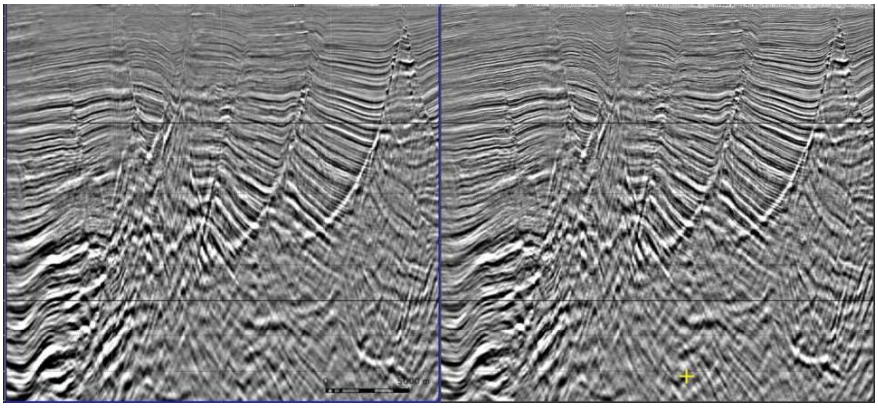

**Figure 5b:** Stack comparison of before amplitude balancing (left) and after amplitude balancing (right). As can be observed, the energy has been balanced out after amplitude balancing was performed.

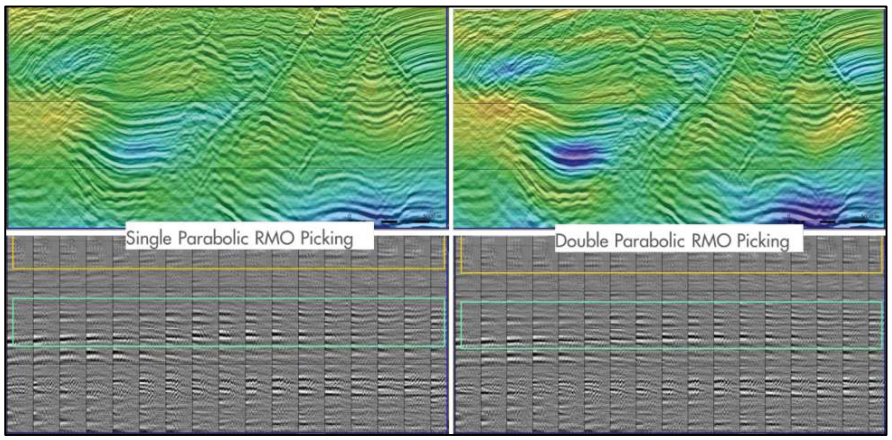


**Figure 6:** Comparison of single parabolic (left) and double parabolic (right) results. Improved details in the double par model and focusing on the gathers.

stacking, and the DSSRT post migration provided a noise filtered version of the BASE RTMIG image. Further post-stack operations like DIP_FLT were applied to better the Signal/Noise ratio.

The RTANG flavor of Reverse Time Migration (RTM) gives you the opportunity to take advantage of the different reflection angles (RFLANG) which is the angle between the source wave field direction and the reflection

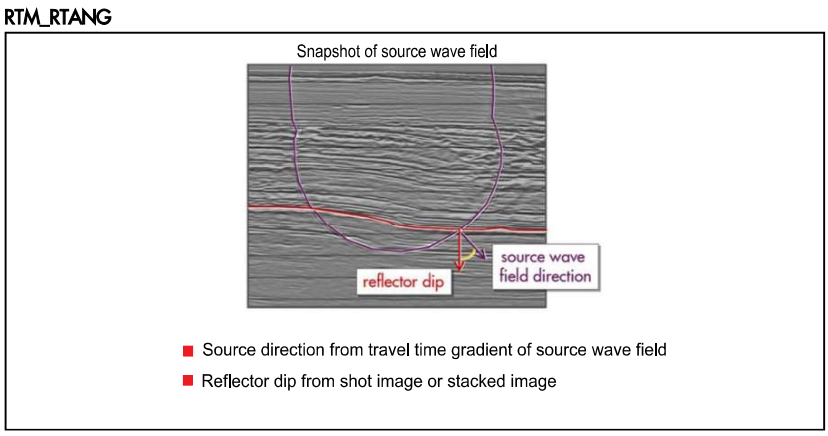


**Figure 7:** description of the RTANG mechanics

dip, (see figure above). Figure 8 below shows the analysis of the different Reflections angles and their corresponding stack quality below.
After careful analysis of the different reflection angles, reflection angle between 3 to 42 degrees gave us an optimum stack quality.

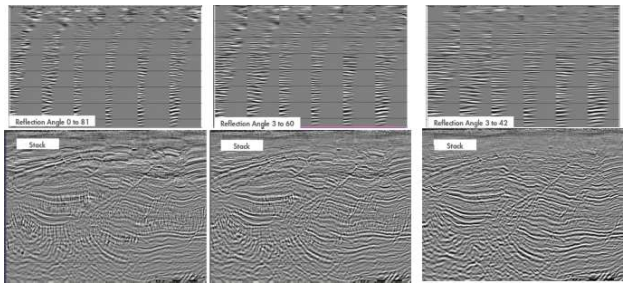


**Figure 8:** Analysis of the different RFLANG for optimum RTM stacking.

## DIP FILTERING

Typically, in a seismic dataset, there could be conflicting dips which are not geologic and often in the opposite direction of the key events (like faults and dipping structures). These conflicting dips as can be seen in the seismic image above (figure 8) creates distortions and reduces the Signal to Noise ratio in the seismic dataset, thereby impacting faults and events interpretations. This was removed from the seismic data using a dip filtering operation developed in-house by shell. For more details, checkout *SEG: A local dip filtering approach for removing noise from seismic depth images Eric Duveneck*, Shell Global Solutions International, (see picture below from Eric's paper)*

**Theory**

In this section, the local dip filter used in this paper is derived. Assume that **k** is a wave-number vector representing a wave-number component of the 3D depth image, and **n** is a unit vector defining a direction in 3D space. If $k_n$ is the component of **k** parallel to **n**,

$$k_n = \mathbf{n} \cdot \mathbf{k} = \cos(\Delta\alpha)|\mathbf{k}|, \quad (1)$$

where $\Delta\alpha$ is the angle between **k** and **n**, then the ratio

$$\frac{k_n^2}{|\mathbf{k}|^2} = \cos^2(\Delta\alpha) \quad (2)$$

can be used to weight any wave-number component of the image according to the angle $\Delta\alpha$ between the wave-number vector **k** and the direction defined by **n**, irrespective of the length of **k**. If we now assume **n** to be a function of space, $\mathbf{n} = \mathbf{n}(\mathbf{x})$, we can no longer compute $k_n$ directly in the wave-number domain. However, we can make use of the fact that – if spatial derivatives of **n** can be ignored – multiplication by $k_n^2$ in the wave-number domain corresponds to the application of a negative second derivative along the direction defined by **n** in the space domain:

$$k_n^2 \leftrightarrow -\frac{\partial^2}{\partial n^2}. \quad (3)$$

• Input volume in the depth and regularly sampled on a rectangular grid with XSSP and YSSP

• The filter that is applied is (cos(dip_angle_difference))^(2*niter), where dip_angle_difference is the dip angle difference between the provided reference dip field and the actual dips present in the depth image.

• For dipsaf=0, zero dip (horizontal) will be assumed as reference dip. In that case, you don't need to provide a dip field.

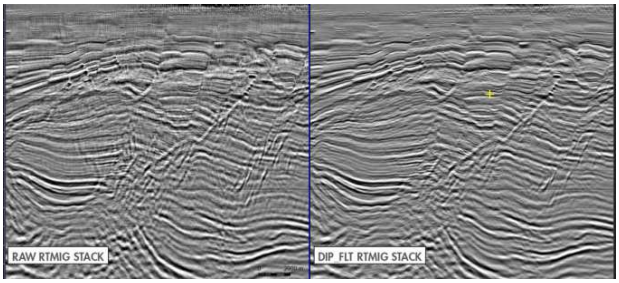


**Figure 9:** Comparison result of the DIP filtering operation. Before application (left) and after application (right).

As can be observed from the figure above, after the application of the dip_flt operation, conflicting dips have been taken out, leading to a more focused and higher signal-noise stack.

## RESULT

A comparison with Sonic logs (DT) also indicated that Model C was an improved Model compared to Model B (see figure 11). For updating, there also existed a Model A, which is an FWI (Full Waveform Inversion) model for shallow combined with legacy velocity for deep. Model B is an additional one pass of TTI with a conventional picking approach.

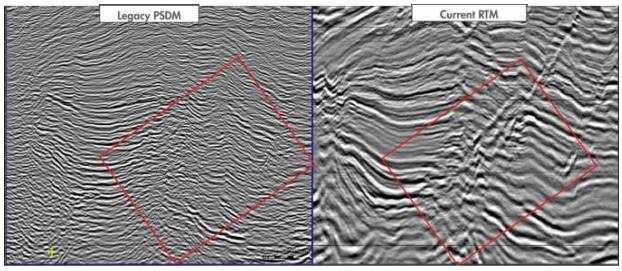


**Figure 10a:** AOI_1 showing a comparison between the legacy PSDM and the new volume (new acquisition, new velocity model, and RTM with RTANG option).

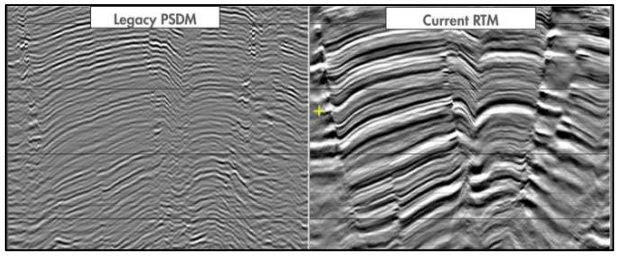


**Figure 10b:** AOI_2 showing a comparison between the legacy PSDM and the new volume (new acquisition, new velocity model, and RTM with RTANG option).

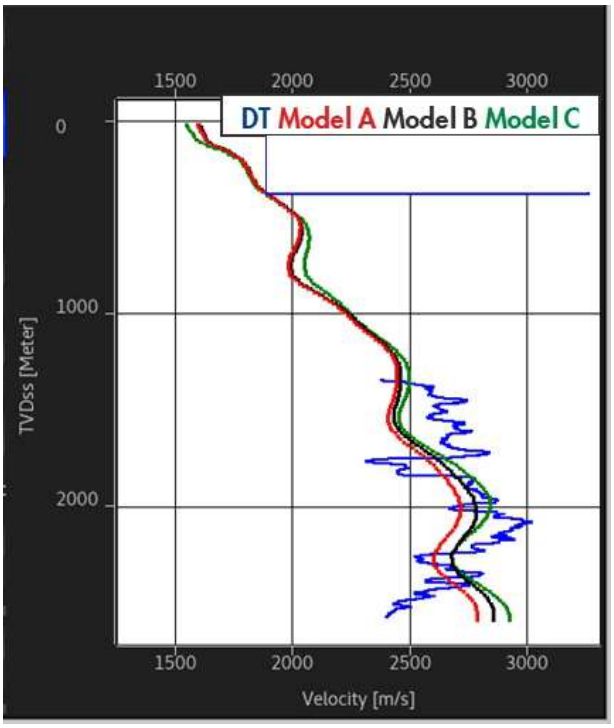


**Figure 11:** A comparison with Sonic logs (DT) also indicated that Model C was an improved Model compared to Model B.

## CONCLUSIONS

Combining the velocity model building approach and the imaging technique gave rise to an improved imaging resulting in a better definition of structural and stratigraphic features within the field. This seismic is aiding well planning and exploration maturation process. This has unlocked a key prospect and have positioned it in the drilling sequence.

## REFERENCES CITED

SEG: A local dip filtering approach for removing noise from seismic depth images: Eric Duveneck*, Shell Global Solutions International.

Shell Technical Report, 2012, 2013, 2015, 2016, 2018, 2020: A Shell Petroleum Development Company of Nigeria, Reports.

Michele L. W. Tuttle, Ronald R. Charpentier, and Michael E. Brownfield, (1999): The Niger Delta Petroleum System: Niger Delta Province, Nigeria, Cameroon, and Equatorial Guinea, Africa. USGS Science for a changing World.